Integrated multiscale simulation of CHP based district heating system

Peifeng Li[a], Natasa Nord[b], Ivar Ståle Ertesvåg[b], Zhihua Ge[a], Zhiping Yang[a], Yongping Yang[a,*]

[a]*School of Energy Power and Mechanical Engineering, North China Electric Power University, NO.2 Beinong Road, Changping District, Beijing, 102206, China*
[b]*Norwegian University of Science and Technology (NTNU), Department of Energy and Process Engineering, NO-7491 Trondheim, Norway*

Abstract

Many studies have been carried out separately on combined heat and power (CHP) and district heating (DH). However, little work has been done considering both the heat source, the DH network and the heat users simultaneously, especially when it comes to the heating system with large-scale CHP plant. For the purpose of energy conservation, it is very important to know well the system performance of the integrated heating system from the very primary fuel input to the terminal heat users. This paper set up a model of 300 MW electric power rated air-cooled CHP plant using Ebsilon software, which was validated according to the design data from the turbine manufacturer. Then, the model of heating network and heat users were developed based on the fundamental theories of fluid mechanics and heat transfer. Finally the CHP based district heating system was obtained and the system performances within multiscale scope of the system were analyzed using the developed Ebsilon model. Several useful conclusions were drawn. It was found that a lower design primary supply temperature of the DH network would give a higher seasonal energy efficiency of the integrated system throughout the whole heating season. Moreover, it was not always right to relate low design supply temperatures to high pump power consumptions and high heat losses in the DH network, since the results showed that the seasonal pump power consumption and the heat loss would decrease with a lower design primary supply temperature. Therefore, from the perspective of seasonal energy efficiency of the integrated system, low temperature DH has an even more bright future compared to just considering the design heat load condition. Both the CHP plant and the low temperature DH network were simulated in detail and integrated, including the part heat load conditions, which is one novelty of this article. The simulation in this paper could be as the basis for the further improvement and optimization of CHP based DH systems.

Keywords: combined heat and power, low temperature district heating, simulation, Ebsilon Professional, heating network, heat users
PACS: x, x, x
2014 MSC: xx-xx

1. Introduction

Nearly every progress of science and technology made by mankind comes along with the excessive exploration of natural resources and serious pollutions. So many changes have been made to the nature on the earth that the fact of energy depletion and global warming is threatening us with, unfortunately, a grave future. One of the most promising ways to dismiss or release this bad situation is to make full use of the remaining energy resources, including renewable energy and fossil fuel, since it is unlikely to stop the development of science or to reduce the daily increasing energy demand of mankind society. In 2013, the global primary energy consumption increased by 2.3%, with an 1.8% acceleration over the year 2012 [1].

Combined heat and power (CHP) can be an energy efficient and environmentally friendly way for energy conversion and utilization, especially when it combines with the customary technology of combined cycle using natural gas [2]. Researches all over the world have been focused on the old but vital technology of CHP. To evaluate the energy conservation characteristics of CHP plants, a series of indicators have been proposed, such as primary energy savings (PES) [3], primary energy rate (PER) [4], trigeneration primary energy saving (TPES) [5], building primary energy

*Corresponding author
Email addresses: lpfncepu@163.com (Peifeng Li), natasa.nord@ntnu.no (Natasa Nord), ivar.s.ertesvag@ntnu.no (Ivar Ståle Ertesvåg), gezh@ncepu.edu.cn (Zhihua Ge), yzprr@163.com (Zhiping Yang), yypncepu@163.com (Yongping Yang)

ratio (BPER) [6], relative avoided irreversibility (RAI) [7] and specific fuel consumption (SFC) [8]. Meanwhile, to bring up the efficiencies of CHP systems, a series of technical measures has been studied with respect to different system types and boundaries [9]. However, most of the recent published studies on CHP are mainly focused on natural gas based small-scale tri-generation systems, such as combined cooling, heat and power (CCHP) [10–12], combined hydrogen, electricity and heat (fuel cell) [13–15], combined renewable energy such as CHP with wind power or solar power [16–20], or biomass [21, 22]. Research on solely conventional CHP with large-scale coal-fired units is relatively insufficient, leading to the reality that the options and parameters of large-scale CHP systems have not been adjusted well with the increasing unit capacities, heat load scales and temperature levels. Besides, with the world-wide hot research and discussion of CO_2 reduction, fossil fuel is becoming not such popular as renewable energy. However, it is impossible to change totally to renewable energy instantly due to present primary energy reserves and infrastructures for countries like China, South Africa, India, Poland, etc. The coal-fired power plants will still be important within foreseeable future. Therefore, intensive study of large-scale coal-fired CHP systems is still an urgent need of top priority in face of current serious energy shortage and environmental degradation.

District heating (DH) is another hot topic in the residential sector, especially under the pressure of energy and environmental problems these years [23]. The fundamental idea of DH is expressed as: to use local fuel or heat resources that would otherwise be wasted, in order to satisfy local customer demands for heating, by using a heat distribution network of pipes as a local market place [24]. Gadd and Werner [25, 26] researched on the heat load patterns shows that normal heat load patterns vary with applied control strategy, season and customer category. Persson and Werner [27, 28] investigated the industrial excess heat utilization in DH and the competitiveness of future DH systems, and concluded that there is no direct barriers for the utilization of industrial excess heat for DH within EU27 and that reduced heat demands in high heat density areas will not be a general barrier for DH in the future. With the goal to decrease the primary return temperature of the heating network, studies have been carried out with respect to the optimization of control strategy of substations which constitute the interface between the distribution network and the heat customers [29–31]. Recently, low temperature DH is becoming a popular research field due to more and more appropriated insulation and airtight building envelopes. Brand and Svendsen [32] studied a typical Danish single-family house connected to DH from the 1970s, the results show that a maximum supply temperature below 60 ℃ would be feasible for 98% of the year with a small refurbishment like changing the windows. Lund et al. [33] defined the concept of 4th generation DH and smart thermal grid. In their definition, low supply temperature, low grid losses and low temperature heat sources are three important features of the future 4th generation DH. Meanwhile, it was also pointed out that the supply temperature as low as 40 ℃ can be used for space heating systems. However, there is a dearth of research related to the optimal low supply temperature of the primary heating network. Besides, all these DH related researches are heating network or heat load and building related studies. Few studies have combined the research with the characteristics of CHP plants, although it is important. On one hand, for instance, a low supply temperature of the DH network (with the constant heat load of the heat users) would result in a large flow and, therefore, high pump power consumption in the heat distribution network. On the other hand, a low supply temperature would come with a lower back pressure of the turbine and, therefore, a higher power output in the CHP plant. The net power output of the overall system is depended on both the two aspects. Therefore, a combined study of DH system concerning simultaneously the characteristics of the CHP plant, the heating network and the heat users is important. A model of the whole heating system is needed for the integrated system analysis.

The objective of this work was to establish and analyze an integrated model of coal-fired large-scale CHP based DH system. Moreover, several important issues with regard to the supply temperature and the losses of the DH network were investigated based on the overall system level. With respect to CHP based DH system, different modes can be adapted, while one energy efficient way is to use the exhaust steam, discharged from the low pressure cylinder (LPC) of the air-cooled turbine, as the heat source, studied in [34]. A brief schematic of the analysed system is shown in Fig. 1. The left part in the figure is the CHP plant, and the right part indicates the DH network with heat users. The exhaust steam from the LPC of the turbine is divided into two parallel flows. One is condensed by air through the air-cooling tower, while the other is condensed by the water from the DH network in the condenser. In this study, the Ebsilon Professional software was used to model the large-scale CHP plant, since it was convenient to carry out the off-design simulation of the power plant, and extended modules could be easily developed in this software platform. Facing the problem that there was no DH pipeline module in Ebsilon, models for both the heat and pressure loss of the pipes in heating networks were set up using the basic theory of heat transfer and fluid

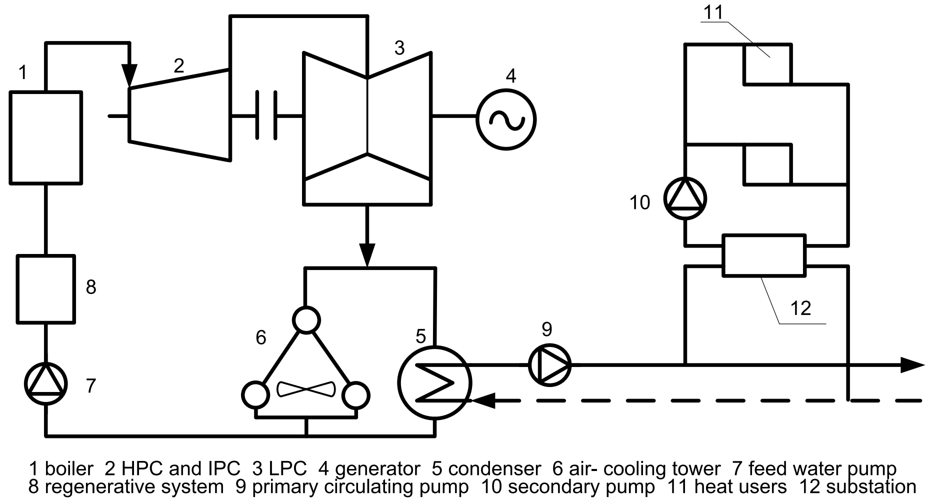

Figure 1: System schematic of CHP based DH system

mechanics. A pipe module was developed within Ebsilon Professional using Pascal programing language. Another module was also developed to estimate the basic characteristics of radiators with heat demand control. These two modules were important to find the relationships among the CHP performance and pipe diameters, heat losses and pump power consumptions. Finally, the integrated CHP based DH system was obtained, and the system performance within multiscale[1] scopes of the system were analysed. The study in the paper should be of interest for designers of DH systems cooperating with CHP plants.

The novelty in this article is that both the CHP plant and the DH network were simulated in detail and integrated. The structure of the further text is as follows: Section 2 will present the description and main specifications of the system studied, and also the evaluation criteria of the system performance. Then, the methodologies of the simulation is presented in Section 3, including the developed heat users, DH pipes and operational issues. Meanwhile, the DH related multiscale performance of the system, including the CHP plant, the heat users and the DH network is presented and analysed in Section 3. Based on the multiscale simulation and analysis, several basic topics with regard to the design supply temperature, the DH pump power consumption and the heat loss rate of the DH network are studied and analysed on the integrated system level in Section 4. Section 5 discusses practical low temperature related considerations, the influence of the terminal temperature of the condenser and the choice of the design specific friction resistance. Finally, some conclusions will be drawn in Section 6.

2. System description and specifications

This paper presents a total energy system study of a coal-fired large-scale CHP-based DH system. Fig. 2 shows the simulation process of the system constructed in Ebsilon software. The detailed theory behind the simulation is given in the next section. In this section, this figure is used to present an overall description of the structure of the integrated system. The left-hand part of Fig. 2 is the CHP plant and the right-hand part indicates the DH network and heat users. The turbine was designed as an air-cooled type[2] and was comprised of the high pressure cyclindar (HPC), the intermediate cyclindar (IPC) and the low pressure cyclindar (LPC). The reason for choosing an air-cooled power plant is that the back pressure level of air-cooled turbines could be easily adjusted for low temperature DH (usually less than 70 ℃), since this type of turbines is equipped with much shorter blades in the LPC than water-cooled ones.

Shown in Fig. 2, The CHP plant studied in this paper was an existing 300 MW power-rated air-cooled plant located in Shanxi Province in China, with the rated back pressure of 0.015 MPa. To be adapted for DH, the back pressure of LPC in operation should be increased. The air-cooling tower (No.6 in Fig. 2) was comprised of 12 air-cooled condensers (ACC), which were separated into three parallel columns with each column consists of four cascaded ACCs. The detailed structures of

[1]Multiscale in this paper means the objects we analysed are of different scales, including the pipe and the user modules, the network and the CHP plant, and also the whole integrated system.

[2]Water-cooled turbine means the turbine designed with the exhaust steam condensed by water. Air-cooled turbine means the turbine designed with the exhaust steam condensed by air.

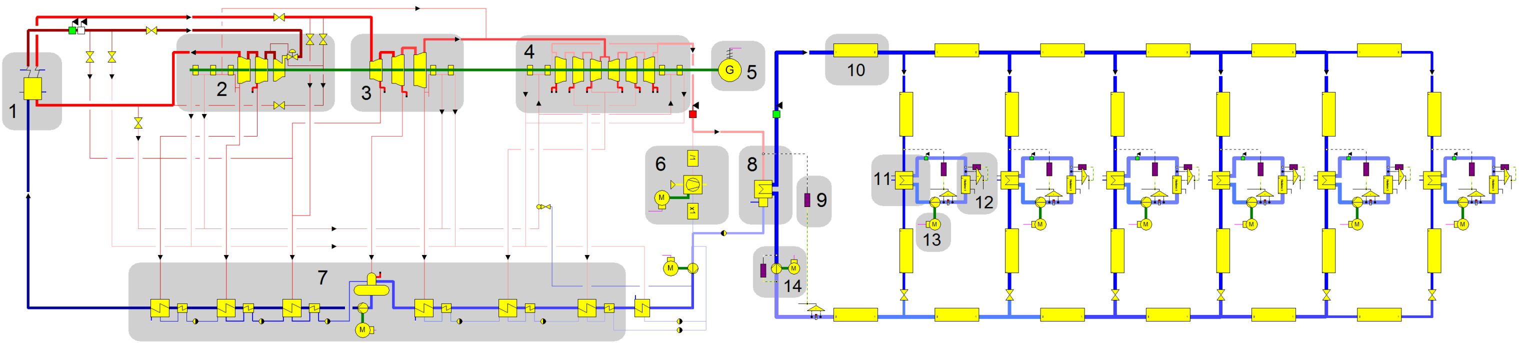

1 Boiler 2 HPC 3 IPC 4 LPC 5 generator 6 air-cooling tower 7 regenerative system 8 condenser/heater for DH netowrk
9 controller 10 pipe module 11 substation 12 heat user module 13 secondary pump 14 primary pump

Figure 2: Technological process of studied integrated system in Ebsilon

the air-cooling tower and ACC could be found in [35, 36] as examples. There was a switching valve before each of the parallel columns to open and close the columns. The switching valves, together with the control of the fan speed of ACCs, were used to control the back pressure of the turbine and the related primary supply temperature of the DH network. The terminal temperature difference of the condenser (No.8 in Fig. 2) was kept at 5 ℃ by changing the back pressure of the turbine in both design and off-design conditions. Number 7 (in Fig. 2) indicates the regenerative system, which consisted of three high pressure heaters, one deaerator and three low pressure heaters. The regenerative system was used to heat the water pumped to the boiler, making use of bleeding steam from the turbine.

The studied DH network was a hypothetical one with six branches (the right-hand part of Fig. 2). Since the structures of the branches were assumed to be the same, only the first substation was labeled. The distance from the condenser at the CHP plant to the first branching point was assumed to be 10 km. And the distance between adjacent branching points was 1 km. For each branch, there was a distance of 100 m from the branching point to the substation. With regard to the heat load of the studied case, since the domestic hot water use is almost constant during the year, inclusion of the domestic hot water will move the duration curve up. It was assumed in this study that there was no domestic hot water supply and the heat load was only considered to be space heating, which is common in China and former Soviet Union countries. The studied space heating load was distributed as six lumped heat users with heating areas of 5.0×10^5 m^2, 1.0×10^6 m^2, 1.5×10^6 m^2, 1.5×10^6 m^2, 1.0×10^6 m^2, 5.0×10^5 m^2, respectively, from the nearest substation to the farthest one. The unit area heating load rate was 60 W/m^2, and design outdoor temperature was -30 ℃. So low outdoor design temperature was chosen to have possibility to extend the plant, since a district heating plant is usually built with long term ideas to include new customers in the future. In total, the maximum heat load rate was 300 MW. The pipeline in DH network is usually separated by the thermal substations as two main parts: primary pipeline and secondary pipeline. Accordingly, there are two kinds of important supply temperatures in DH networks: primary supply temperature and secondary supply temperature.

Issues of the integrated systemin will be presented in Section 4. The studies of the integrated system were based on the premise that the inlet steam parameter of the HPC of the turbine was kept constant and identical with the THA condition. Energy efficiency (Eq. 1) was used to indicate the energy dissipation character of both the CHP plant and the integrated system.

$$\eta_t = \frac{\dot{Q} + P_e}{\dot{Q}_i} \tag{1}$$

where η_t and $\dot{Q}_i$ indicate the energy efficiency and the rate of input energy of the CHP plant, respectively. For the calculation of $\dot{Q}_i$, the boiler efficiency in CHP plant was assumed to be constant at 0.92, which do not affect the total system character since the inlet steam parameter of the turbine was kept constant in the simulations. $\dot{Q}$ denotes the rate of heat output of the system discussed. Three terms were used in the further text - the CHP plant efficiency, the overall

Table 1: Basic design parameters of the turbine for THA condition

Parameters (unit)	Value	Parameters (unit)	Value
Unit type (-)	NZK300-16.7/538/538	Reheated steam flow (kg/h)	7.84×10^5
Rated power capacity (MW)	300	Reheated steam temperature (℃)	538
Main steam flow (kg/h)	9.52×10^5	Reheated steam pressure (MPa)	3.33
Main steam temperature (℃)	538	Stages of regenerative system (-)	6
Main steam pressure (MPa)	16.7	Back pressure (kPa)	0.015

efficiency and the seasonal efficiency. For the CHP plant efficiency (energy efficiency of the CHP plant), $\dot{Q}$ refers to the heat rate transferred from the CHP plant to the DH network. For the overall efficiency (energy efficiency of the integrated system), $\dot{Q}$ refers to the total heat load (the rate of heat supplied to the users). In order to investigate into the total energy performance of the integrated system in the whole heating season, the seasonal energy efficiency (η_{av}) is defined as the sum of the net power output and heat load divided by the sum of the energy input of the CHP plant during the whole heating season (kWh/kWh). Analysis and comparison of the overall efficiency and the seasonal efficiency are one of the novelty in this paper. P_e indicates the electric power output of the system discussed. For the CHP plant efficiency, it is the turbine power output minus the self used power in the CHP plant. For the overall efficiency, it is the turbine power output minus all the self used power including the pump power consumption in the DH network.

3. Methods

Simulations of the integrated system were implemented on the platform of Ebsilon Professional software, which is specialized in power generation fields and is used to design, simulate and optimize thermodynamic cycle processes in power plants. The most satisfactory advantage of EBSILON is that it can simulate the part-load (off-design) conditions [37]. Since there was neither radiator module nor pipe module in Ebsilon, two more modules for DH were developed. For the thermodynamic properties of water and steam at any state, the IAPWS Industrial Formulation 1997 [38] was used. With regard to the precision of the simulated results, 10^{-7} was used as the criterion to evaluate the convergence of the equation based matrix[3].

There are two calculation modes in Ebsilon, design mode and off-design mode. Both of them are based on energy and mass flow balances. The design mode is used to construct the physical layout of the components in the studied system and assign the design parameters, such as temperature, pressure, flow and efficiency. Thus the heat-transfer areas of the heat exchangers, the flow cross-sectional areas of the turbine wheels and channels will be fixed. The off-design mode is used to give the answer to what-if problems based on the fixed design structures according to basic off-design formulae and characteristic curves, such as the Stodola equation and efficiency curves etc.

To investigate into the integrated characteristics of the whole system, two main parts are considered in this section. One is the CHP plant, the other is the heating network. The heat load feature was included in the heating network part. Both the two main parts could be simulated and validated in Ebsilon software. However, in order to carry out the simulation of the heating network, radiator module and pipe module have to be developed to realize the hydraulic and heat loss calculation of pipelines and to model the heat load characteristics of heat users. The novelty in this article is that both the CHP plant and the DH network were simulated in detail and integrated.

3.1. CHP plant simulation and validation

The 300 MW CHP plant was constructed using the built-in modules in Ebsilon (see Fig. 2) according to the design data of turbine heat-acceptance (THA) condition with the main parameters presented in Table 1. For off-design mode, the Stodola equation [39] was adopted in the turbine calculation, and the Rabek method [40] was used in regenerative heater calculation. The modules of the boiler, the turbines and the condenser are assumed to be adiabatic. The efficiencies of the stages in the turbine were fitted with the design data provided by the manufacturer. As an example, Fig. 3 shows the fitted relative efficiency curve of the last stage group in the LPC. Here, 'relative' means the ratio of the value from off-design mode to that of the design mode.

[3] 10^{-7} is the maximum relative deviation in the present iteration from that in the last iteration when solving the matrix

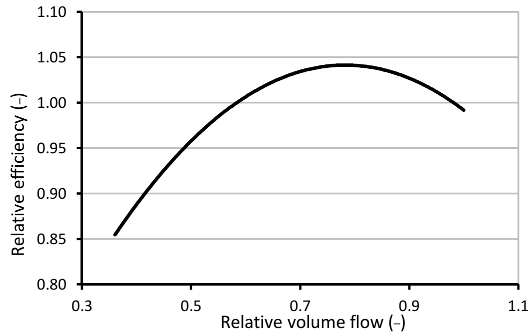

Figure 3: Relative efficiency curve of the last stage group in LPC

Table 2: Main input parameters of the CHP unit under part-load conditions

Part-load conditions	100% THA	75% THA	50% THA	40%THA	30%THA
Flow rate (t/h)	951.94	693.12	462.22	377.74	295.18
Main steam pressure (MPa)	16.70	16.70	11.59	9.54	7.51
Reheat steam pressure (MPa)	3.33	2.48	1.70	1.39	1.08
Temperature (℃)	538	538	538	538	538

To validate the off-design simulation result of the CHP plant, a comparison between the simulated part-load power output and the tested part-load power output was presented. The tested part-load data was provided by the manufacturer of the turbine unit. The main steam parameters for different part-load conditions are shown in Table 2, and the comparison curve is shown in Fig. 4a.

Table 2 and Fig. 4a show that the power output decreased with the decrease of the main steam flow rate and pressure. For part-load conditions, the power output deviations increased when the load was lower. The largest relative deviation occurred at 30% THA condition (4.1%), while the deviation at 100% THA condition approached zero. The simulated part-load power output of the CHP plant was basically consistent with the design value.

Since one of the most important variable of the study was the back pressure of the turbine, it was necessary to look into the off-design characteristics with different back pressures to further validate the power plant simulation. Fig. 4b shows the simulation results of the CHP plant with regard to the variation of the back pressure. The power output of the turbine increased when the back pressure became lower, except for very low back pressure conditions. The simulation result of Fig. 4b was consistent with the results previously obtained in [41].

Since the off-design calculations mentioned above were consistent with the design data and previous studies, the simulation model of the CHP plant was considered to be acceptable.

3.2. Heat user model

The heat load in this study was only space heating, without any domestic hot water considerations. Domestic hot water use is almost constant during the year, inclusion of the domestic

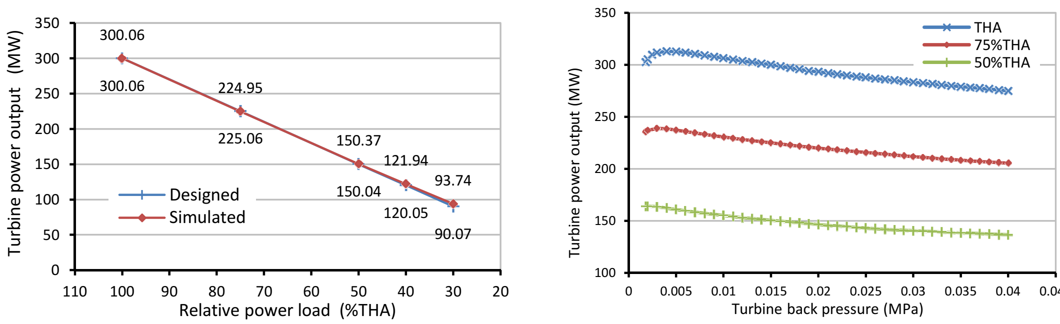

(a) Part-load conditions

(b) Back pressure variations

Figure 4: Off-design simulation of the CHP plant

hot water will move the duration curve up. Besides, heating systems with only space heating heat load is typical and relevant for DH studies in China and former Soviet Union countries. For space heating, heat released at the heat users is basically related to the characteristics of the radiators. Considering that there is no built-in radiator module in Ebsilon, a mathematical model of radiator was set up and a radiator module was developed to simulate the characteristics of heat users in the DH network. In the further text, the mathematical model and the validation of the heat user model is presented.

3.2.1. Mathematical model

The heat transfer process of the radiators is theoretically expressed by the following two equations:

$$\dot{Q} = k_r \cdot A_r \cdot \triangle T_{m,r} \tag{2}$$

$$\dot{Q} = \dot{G} \cdot \triangle h \tag{3}$$

where $\dot{Q}$, k_r, A_r, $\triangle T_{m,r}$, $\dot{G}$, $\triangle h$ represent the rate of heat, the heat transfer coefficient, the heat transfer area, the mean temperature difference, the water flow rate and the enthalpy drop of the water in the radiator, respectively.

$\triangle T_{m,r}$ is calculated as the logarithmic mean temperature difference, expressed as

$$\triangle T_{m,r} = \frac{T_{i,r} - T_{o,r}}{\ln \frac{T_{i,r} - T_n}{T_{o,r} - T_n}} \tag{4}$$

where $T_{i,r}$, $T_{o,r}$, T_n are the inlet temperature of the radiator, the outlet temperature of the radiator and the indoor temperature needed, respectively.

The heat transfer coefficient of the radiator, k_r, is defined as

$$k_r = a \cdot (\triangle T_{m,r}/[\mathrm{K}])^b \tag{5}$$

where a and b are the coefficients of the radiator. In the study of this paper, the values of a and b were set as 1.38 and 0.26, respectively [42].

When the outdoor temperature changes, the heat load will also change accordingly. The relative heat load can be expressed as

$$\frac{\dot{Q}}{\dot{Q}_{max}} = \frac{T_n - T_a}{T_n - T_{a,min}} \tag{6}$$

where T_a, $T_{a,min}$ and $\dot{Q}_{max}$ represent the ambient temperature, the lowest calculated ambient temperature and the maximum heat load, respectively.

Based on the theory above, a radiator module was developed within the Ebsilon platform using Pascal programming language.

3.2.2. Analysis and validation of the heat user model

To test the characteristics of the heat user model, a set of sensitive analysis was conducted with the results shown in Figs. 5 - 6.

Fig. 5 presents radiator characteristics with different design supply temperatures (design $T_{i,r}$). The design supply temperatures in Figs. 5a - 5b were set from 55 ℃ to 95 ℃. The design supply temperatures in Fig. 5c were set as 55 ℃ and 85 ℃ for comparison. Fig. 5a shows the off-design characteristics of the radiator with different operational flow rates under different design supply temperatures. When increases the flow rate, the rate of heat increased with a gradually reduced slope. A lower design supply temperature gave a smaller slope. However, the radiator with a lower design supply temperature required a much larger heat transfer area, as shown by Fig. 5b. The heat transfer area with the design supply temperature of 60 ℃ was set as the reference base with regard to the relative area in Fig. 5b. Fig. 5c presents a comparison of radiator off-design characteristics with two different design supply temperatures. It was found that a lower design supply temperature or a higher operational supply temperature (operational $T_{i,r}$) gave a much more linear-like performance. This would enable easier heat load control in operation [24].

In order to investigate into the heat user characteristics influencd by the pattern of radiators, different b values were used for the radiator analysis shown by Fig. 6. Fig. 6a shows that a larger b value tends to give a more linear relationship between rate of heat and flow rate. Meanwhile, with a larger b value, the heat transfer area of the radiator decreased dramatically, especially within the range of (0, 1) (see Fig. 6b). The reference base for the relative heat transfer area in Fig. 6b

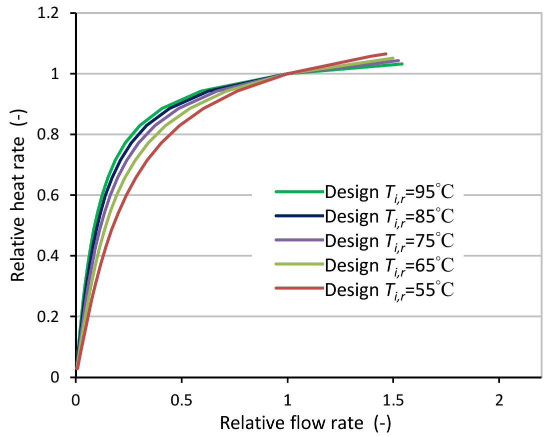

(a) design $T_{i,r} = 55 - 95$°C

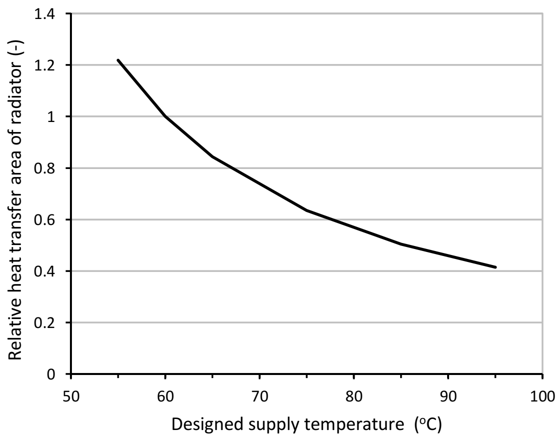

(b) design $T_{i,r} = 55 - 95$°C

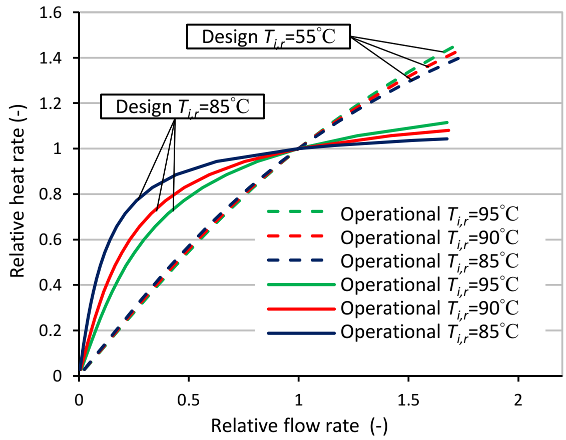

(c) design $T_{i,r} = 55$°C, 85°C

Figure 5: Radiator characteristics with different design supply temperatures

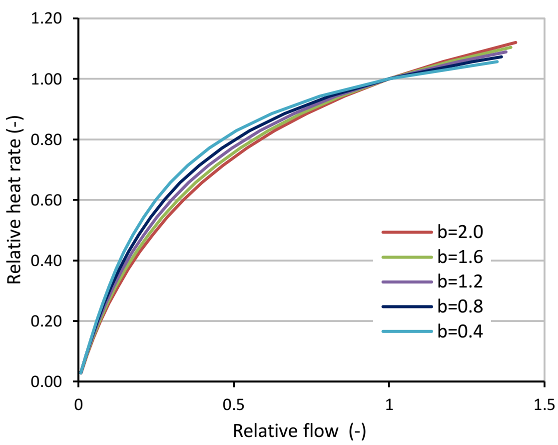

(a) Rate of heat with different b values

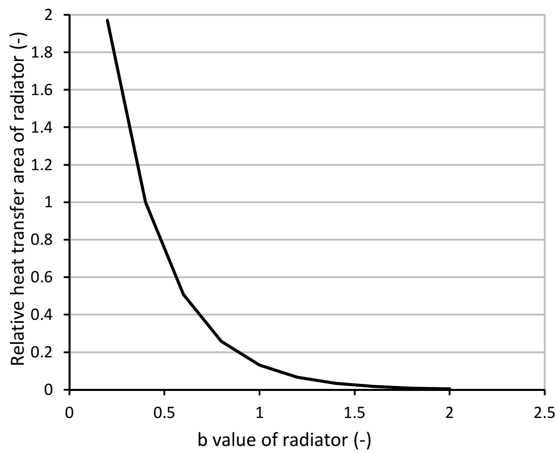

(b) Heat transfer area with different b values

Figure 6: Radiator characteristics with different a or b values

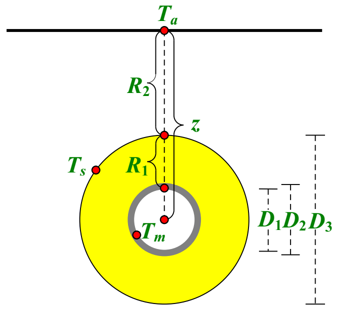

Figure 7: Geometry of the pipe buried underground

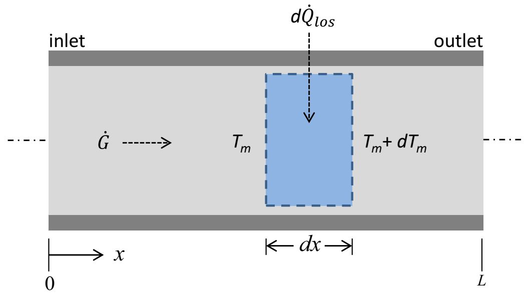

Figure 8: Calculation model for the temerature distribution along pipe

was the area when $b = 0.4$. With respect to the influence of a value of radiators, its variation only contributed to different design heat transfer areas of the radiators. A larger a value gave a smaller heat transfer area of the radiator, with similar trend as that in Fig. 6b.

To validate the result of the radiator module, a numerical interation calculation in Microsoft Excel was carried out according to Eqs. 2 - 3. The result was compared with that obtained from the developed Ebsilon module, which showed a high consistency. The inlet parameters were given and the relative difference of the outlet temperature was 0.01%. Besides, similar tendancy in Fig. 5a was also found in Literature [43].

3.3. Model of the heat and pressure loss in the heating network

Similar to the radiator module, a pipe model was also necessary for the simulation of the pipelines, which could do both the pipe sizing calculations and the pressure and heat loss calculations. Detail analysis of the heat loss and pressure loss of the DH network is the novelty of this article. The geometry of the developed pipe module buried underground is shown by Fig. 7. The upper black line indicates the ground surface and the yellow part indicates the thermal insulation casing.

3.3.1. Mathematical model of the pipe in heating network

With regard to the hydraulic analysis of the pipe module, the pressure drop of water flow in DH pipes is calculated according to the Darcy–Weisbach equation, which can be expressed as

$$\triangle P = f \cdot \frac{\rho v^2}{2D_1} \cdot L = R \cdot L \tag{7}$$

where $\triangle P$, f, ρ, D_1, v and L are, respectively, the pressure drop, the friction factor, the density of water, the inner diameter of pipe, the water velocity and the length of pipe. The pressure drop was calculated by considering only the frictional resistance along the pipe. The local resistance was not considered in this study. The pipe sizing calculation and analysis were carried out to investigate the influence of specific frictional resistance, R, to the overall system performance. The water velocity was calculated from the mass flow rate, $\dot{G}$. The friction factor was calculated by

$$\frac{1}{\sqrt{f}} = -2.0 \cdot \log \left(\frac{K/D_1}{3.7} + \frac{2.51}{\mathrm{Re} \cdot \sqrt{f}} \right) \tag{8}$$

where K is the roughness of the inner pipe surface, and Re is the Reynolds number of the pipe flow.

In order to calculate the thermal resistance of pipe casing, geometry of buried pipe is considered shown by Fig. 7, in which the pipe casing is considered as a cylinder [44]. Neglecting the interfacial contact resistances and treating the thermal conductivities as constants in the derivation, the overall heat transfer coefficient of the insulated pipe is expressed by

$$U = \left[\frac{D_3}{D_1 \cdot h} + \frac{D_3 \cdot \ln\left(D_2/D_1\right)}{2 \cdot \lambda_p} + \frac{D_3 \cdot \ln\left(D_3/D_2\right)}{2 \cdot \lambda_c} \right]^{-1} \tag{9}$$

where U, D_2, D_3, h, λ_p and λ_c represent the heat transfer coefficient of insulated pipe, the outer diameter of pipe, the outer diameter of insulation, the convection heat transfer coefficient of the inner pipe surface, thermal conductivity of pipe and thermal conductivity of pipe casing, respectively. For the flow with small to moderate temperature differences between the fluid and the environment, the following convection correlation is available for the calculation of h (the Gnielinski correlation [44]).

$$\mathrm{Nu} = \frac{h \cdot D_1}{\lambda_w} = \frac{(f/8) \cdot (\mathrm{Re} - 1000) \cdot \mathrm{Pr}}{1 + 12.7 \cdot (f/8)^{1/2} \cdot \left(\mathrm{Pr}^{2/3} - 1\right)} \tag{10}$$

where λ_w, Nu and Pr are the thermal conductivity of water, the Nusselt number and the Prandtl number, respectively. The thermal resistance of the insulated pipe as a cyclinder (R_1) is

$$R_1 = \frac{1}{U \cdot \pi \cdot D_3 \cdot L} \tag{11}$$

The rate of heat from the surface of pipe casing to the ground surface (see Fig. 7) was calculated as [44]:

$$\dot{Q}_{los} = S \cdot \lambda_0 \cdot (T_s - T_a) \tag{12}$$

where $\dot{Q}_{los}$, λ_0, T_s and S represent the rate of heat loss, the thermal conductivity of the soil, the surface temperature of the pipe casing and the shape factor of the pipe and soil, respectively. The pipe and soil were treated as a horizontal isothermal cylinder of length L buried in a semi-infinite medium, and the shape factor was calculated as

$$S = \frac{2 \cdot \pi \cdot L}{\cosh^{-1}\left(2 \cdot z/D_3\right)} \tag{13}$$

where z is the buried depth of the pipe centerline. Thus, the thermal resistance of the soil over the pipe casing, R_2, is

$$R_2 = \left(S \cdot \lambda_0\right)^{-1} \tag{14}$$

In order to get the temperature distribution along the pipe, a heat transfer model along the pipe was built as shown in Fig. 8. For the control volume in the pipe, the heat loss is expressed as:

$$d\dot{Q}_{los} = \dot{G} \cdot c_p \cdot dT_{m,p} \tag{15}$$

while the rate of heat loss is also expressed by the heat transferred through the pipe casing as

$$d\dot{Q}_{los} = \pi \cdot D_3 \cdot U \cdot (T_s - T_{m,p}) \cdot dx \tag{16}$$

Eqs. 15 and 16 are combined as

$$\frac{dT_{m,p}}{dx} = \frac{\pi \cdot D_3 \cdot U \cdot (T_s - T_{m,p})}{\dot{G} \cdot c_p} \tag{17}$$

The soil surface temperature is assumed to be equal to the ambient temperature, the heat transferred through R_1 is equal to the heat transferred through R_2 (see Fig. 7), and the following equation is readily obtained

$$\dot{Q}_{los} = \frac{T_{m,p} - T_s}{R_1} = \frac{T_s - T_a}{R_2} \tag{18}$$

and can be rewritten as

$$T_s = \frac{T_{m,p} \cdot R_2 + T_a \cdot R_1}{R_1 + R_2} \tag{19}$$

Table 3: Pre-set design parameters of the pipe for performance analysis

Length (m)	Flow (t/h)	Ambient temperature (°C)	R range (Pa/m)	Insulation thermal conductivity ($W/(m \cdot K)$)	Insulation thickness (m)	Soil thermal conductivity ($W/(m \cdot K)$)
1000	1000	-30	[40, 80]	0.03	0.2	1.5

Combining Eq. 17 and Eq. 19, the differential form of temperature distribution along the pipe is obtained as

$$\frac{dT_{m,p}}{dx} = \frac{\pi \cdot D_3 \cdot U \cdot \left(\frac{T_{m,p} \cdot R_2 + T_a \cdot R_1}{R_1 + R_2} - T_{m,p} \right)}{\dot{G} \cdot c_p} \tag{20}$$

When noticing that $T_{m,p} = T_{i,p}$ at $x = 0$ and integrating Eq. 20, the temperature distribution along the pipe is obtained as

$$\ln \frac{T_{m,p} - T_a}{T_{i,p} - T_a} = -\frac{\pi \cdot D_3 \cdot U}{\dot{G} \cdot c_p} \cdot \frac{R_1}{R_1 + R_2} \cdot x \tag{21}$$

where $T_{i,p}$ is the inlet temperature of the pipe. Besides, the heat loss rate along the pipe is expressed as

$$\dot{Q}_{los} = \dot{G} \cdot c_p \cdot (T_{i,p} - T_{o,p}) \tag{22}$$

where $T_{o,p}$ is the outlet temperature of the pipe calculated by Eq. 21 with $x = L$.

Finally based on the theory above, a pipe module was implemented in Ebsilon.

3.3.2. Analysis and validation of the DH pipe model

Pre-set values of the pipe module is shown in Table 3. In order to give a general description of the characteristics, several curves was given from Fig. 9 to Fig. 12. Results from simulations in design mode are shown in Figs. 9 - 10. Fig. 9 is the pipe sizing result with different flow rate and R range. Fig. 10 is the relationship of the heat loss rate versus insulation thickness. Figs. 11 and 12 shows results from simulations in off-design mode. Fig. 11 is the pressure and temperature drops with different operational flow rates, while performance with different operational supply temperatures is shown by Fig. 12.

Fig. 9a shows that a larger flow rate was delivered with a wider pipe and the design diameter of the pipe would increase stepwise with the increase of flow. Accordingly, the heat loss rate would decrease. The reason for the general decrease of the heat loss rate was that a larger flow rate with wider pipe gave a bigger Re value and a smaller f value (Eq. 8). A smaller f value meant a bigger heat transfer coefficient (Eq. 10) and a smaller heat loss. Since the typical range of the R value for pipe sizing was 50-200 Pa/m in Europe [24], which was different from that in China, 40-80 Pa/m [45], an investigation of different R range was also necessary. The pipe sizing process was generally based on Eq. 7 with the detailed knowledge shown in most text books [45]. It can be seen from Fig. 9a that the design pipe diameter was smaller for the R range of 80-120 Pa/m than that of 40-80 Pa/m with regard to the same flow rate. The relative heat loss in Fig. 9a meant the ratio of heat loss to heat delivered by the pipe. The lower R range with wider pipes tended to give a smaller relative heat loss with regard to the same flow. The reason was that a lower R range meant a smaller velocity and smaller heat transfer coefficient, although the heat transfer area was larger for a wider pipe.

Fig. 9b is the relationship between heat loss rate and design diameter. For a specified nominal diameter, the heat loss rate increased due to the increased flow rate and velocity. For an adjacent wider pipe, the heat loss rate would start at a relatively lower level but ends up at a higher value. The reason why an adjacent wider pipe starts at a lower heat loss rate was that the pipe dimensioning was conducted by a range of R and the lower value within R range was preferentially selected. That is to say, an adjacent wider pipe start with a higher flow rate but lower R value. A lower R value meant a lower velocity of the flow and a smaller Re value, resulting in a smaller heat transfer coefficient (Eq. 10). For the general trend, Fig. 9b shows that wider pipes gave larger heat losses. However, although the absolute value of heat loss rate was bigger for wider pipes, the relative value of heat loss rate of wider pipes was smaller, as previously analysed in Fig. 9a.

Fig. 10 depicts the influence of insulation thickness to heat loss rate. The heat loss rate could be reduced by increasing the insulation thickness. However, e.g. in the studied case, the descending trend would be largely reduced when the insulation thickness became larger. A similar curve of heat loss versus insulation thickness can be found on Page 322 in [24].

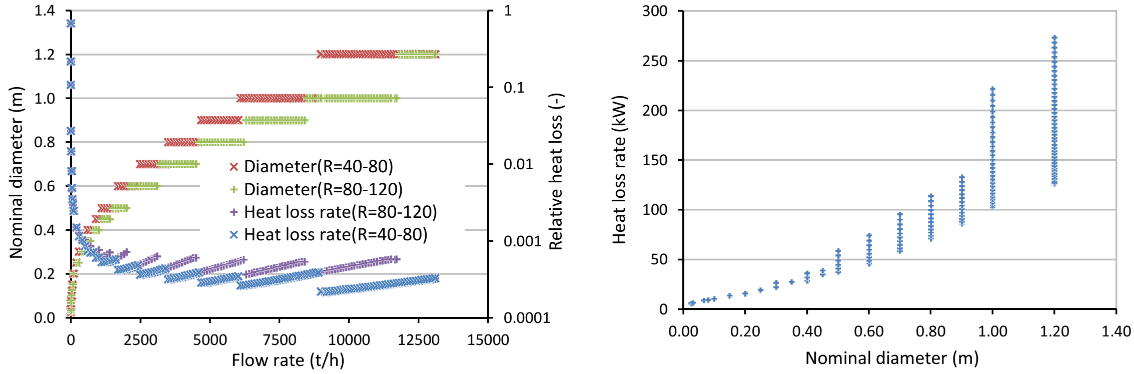

(a) Heat loss and diameter versus flow rate

(b) Heat loss rate versus diameter

Figure 9: Pipe sizing test of the pipe module with different flow rate and R ranges

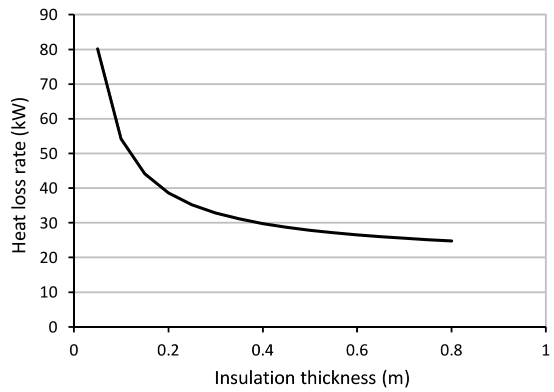

Figure 10: Heat loss of the pipe module with different insulation thickness

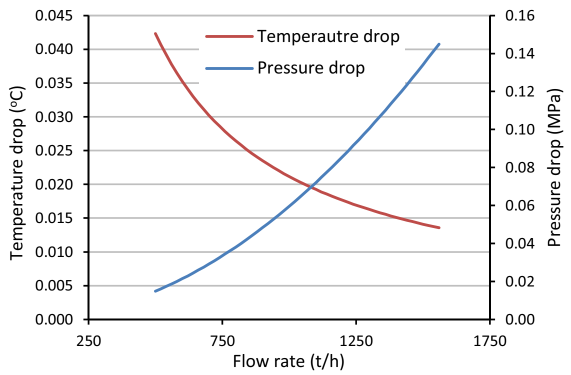

Figure 11: Off-design characteristics of pipe module with different flow rates

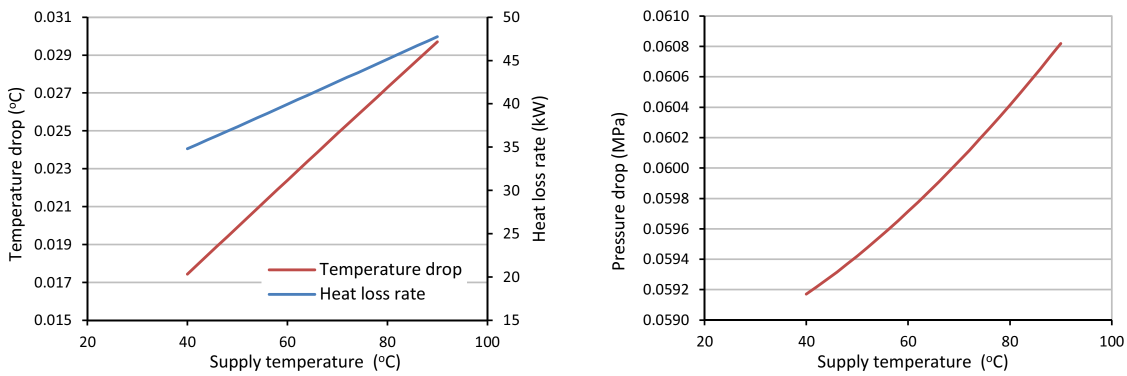

(a) Heat loss rate and temperature drop (b) Pressure drop

Figure 12: Off-design characteristics of pipe module with different inlet temperatures

Fig. 11 is the off-design characteristics of the pipe module with different flow rates. With the increase of flow rate in off-design calculation, the pressure drop would increase and the temperature drop would decrease to different extents. Fig. 12 presents the off-design performance of the pipe with different inlet temperatures. With a higher inlet temperature, the temperature drop and heat loss rate of the pipe increased (see Fig. 12a). This gives us an illumination that low temperature DH could reduce the heat and temperature losses. Fig. 12b shows that the pressure drop of the pipe would also increase, though not much, with a higher inlet temperature. The slight increase of the pressure drop in Fig. 12b was mainly caused by the expansion of water at higher temperatures. With expansion, the water velocity and the friction factor would be increased a little bit, causing the increase of pressure drop. The results presented by Fig. 11 and Fig. 12b were consistent with the fact expressed by Eq. 7.

To further validate the simulation result of the developed pipe module, heat loss calculation using Logstor pipe calculator [46] was conducted for comparison. The results did not deviate from each other more than what is acceptable. For a 450 mm nominal diameter pipe with a pipe casing diameter of 710 mm and an inlet temperature of 80 ℃, the heat loss rate calculated by the Logstor calculator was 40.6 W/m. The simulation result from the developed pipe module in this study was 42.2 W/m. The simulation result by the developed pipe module was slightly higher. Many factors can contribute to this deviation, including different water properties or different heat transfer correlations.

3.4. Heating network

After the development and analysis of the heat user and DH pipe modules, the DH network could be constructed in Ebsilon, as shown by the right part of Fig. 2. The thermal substations in the studied system were all indirectly connected ones. That is to say, the heat exchanging facilities in the thermal substaitons are all dividing wall type heat exchangers, which seperate the water in the primary DH network from that in the secondary DH network. The lower terminal temperature difference of the heat exchangers in the substations was assumed to be 5 ℃. That is to say, the outlet temperature of the heat exchangers in substations was set as 5 ℃ above the outlet temperatures of the heat users. The temperature drop of the radiators at the heat users was set as 10 ℃ for design conditions.

As for the control method of the heating network, four basic measures were taken to keep it running steadily including heat load control, flow control, differential pressure control and supply temperature control. Heat load control is to control the heat released by the radiator to the room space using thermostatic valves. Flow control is to control the primary flow rate that goes into the thermal substations using control valves. Differential pressure control is to guarantee the available pressure difference at the most peripheral substation. Supply temperature control is to control the energy input of the heat source to make the primary supply temperature go as pre-set values. The detailed theory behind the four basic control methods is illustrated in [24].

Key characteristics of the heating network are shown in Fig. 13. Fig. 13a shows the relationship among the heat loss rate, the pump power and the ambient temperature of the DH network. With the increase of ambient temperature in off-design mode, the heat load rate and flow rate would decrease accordingly (Eqs. 6 and 3). Meanwhile, the heat loss rate and pump power would also decrease. For the same ambient temperature, the low designed primary supply temperature (55 ℃) would induce a higher flow and therefore higher heat losses and higher pump power compared

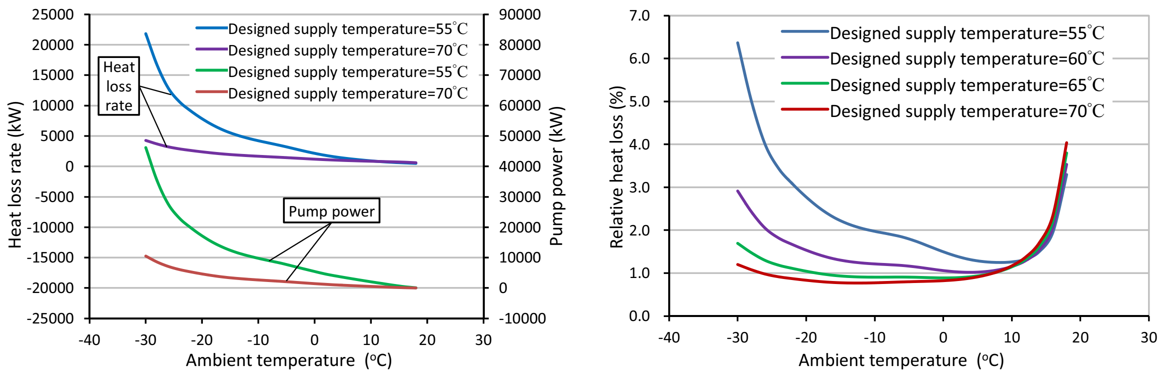

(a) Heat loss rate and pump power

(b) Relative heat loss

Figure 13: DH network characteristics

to that of high designed primary supply temperature (70 ℃). Fig. 13b is the off-design relative heat loss of the discussed heating network with different design supply temperatures. Relative heat loss means the ratio of total heat loss to heat transferred into the heating network. With regard to different design supply temperatures of the heating network, the relative heat loss curves show the same trend but with different levels. For the same heat load, lower designed primary supply temperature causes higher network heat loss. The reason was that, for the lower designed primary supply temperature, the mass flow rate will increase.The increased mass flow rate will require the bigger designed pipe diameter. The bigger pipe diameter will induce bigger cover area of the pipe. A bigger pipe area in contact with the ground will induce higher heat losses.

Fig. 13b also shows that the relative heat loss was high with lower ambient temperatures. With the increase of ambient temperature, there came a trade-off of two effects. One effect was that the relative heat loss would decrease due to smaller flow velocity and smaller temperature difference between internal flow and ambient temperature. The other effect was that the relative heat loss went up dramatically when the heat load approached zero with still none-zero heat loss. Generally, when the ambient temperature increased to a certain level (about 10 ℃ in Fig. 13b), the second effect played a dramatic leading role and the relative heat loss was increased sharply. For high ambient temperature conditions, e.g. when the ambient temperature is above 10 ℃ ,space heating is mostly not needed, the results after 10 ℃ in Fig. 13b might be less relevant. This indicate an important conclusion: at the very low heat load or when the outdoor temperature is high, the network heat losses will be high compared to the load. This is one of the reason why district heating might be not preferable for very low load area.

3.5. Operational issue for the whole heating system

A duration curve of ambient temperature in the heating season is the basis of heat load calculations, and could be expressed with an adequate approximation as Raiss equation [47, 48]as

$$\frac{T_{a,st} - T_a}{T_{a,st} - T_{a,min}} = 1 - \sqrt[3]{\frac{\tau}{\tau_0}} + \left(\frac{\tau}{\tau_0}\right)^2 \cdot \left(1 - \sqrt{\frac{\tau}{\tau_0}}\right) \tag{23}$$

where $T_{a,st}$, τ and τ_0 represent the ambient temperature when the heating season starts, the time and the duration of the heating season, respectively. For each hour in the heating season, there is an ambient temperature and a heat load. With $T_{a,st}$ set as 10 ℃, T_n set as 20 ℃ and τ_0 set as 2880 h, the duration curve used in this work is presented by Fig. 14. To get the total energy consumption of the integrated heating system during the whole heating season, the discrete sum-up calculation of energy consumptions in every hour is carried out, which is considered to be the substitution for consecutive integration.

In this study, the whole heating season is divided into 40 intervals by the ambient temperature ranging from -30 ℃ to 10 ℃. For each interval, a duration time could be obtained by Eq. 23. Thus, the heat load duration curve (Fig. 14) was interpreted and simplified as Fig. 15.

Supply temperatures (primary supply temperature and secondary supply temperature) are of great importance to the overall system performance. Normally, the supply temperatures of primary and secondary networks in operation are always controlled to be lower with the increase of ambient temperature. With regard to the heat exchanger for the heating network, which actually servers as a condenser in the CHP plant, its terminal temperature difference is kept as 5 ℃ by changing the back pressure of the turbine in both design and off-design conditions. That is to say, the

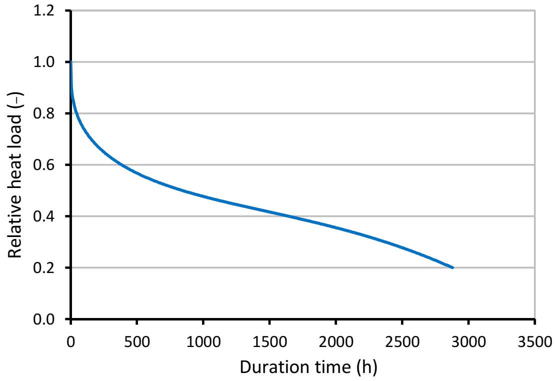

Figure 14: Heat load duration curve of the case studied

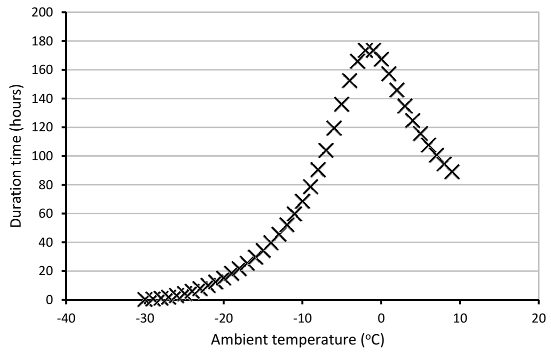

Figure 15: Time duration distribution of the whole heating season with different ambient temperatures

saturated temperature of the steam discharged from the turbine is 5 ℃ higher than the primary supply temperature of the DH network.

4. Analysis and results of the overall system

In order to obtain the overall performance of the integrated scale of the system, several topics are discussed below. Generally, the supply temperature, the pump power consumption and the heat loss of the heating network with regard to different design and operational conditions were studied. Some key figures were selected and analysed as the simulation results of these topics.

4.1. Supply temperature in design conditions

The primary and secondary supply temperatures of the DH network are of great importance for both the design and off-design conditions. The analysis in this subsection only deals with design conditions, while the off-design conditions were discussed in Section 4.2.

For design conditions, different primary and secondary supply temperatures would give out different system designs, with different overall efficiency levels. Fig. 16 shows the system energy

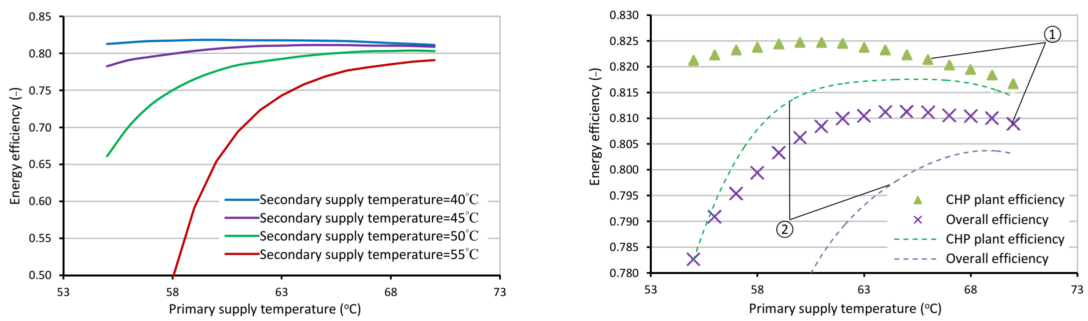

(a) Overall efficiency (b) With different secondary supply temperatures

① Secondary supply temperature=45℃; ② Secondary supply temperature=50℃

Figure 16: System energy efficiency curves under design conditions with different design supply temperatures

efficiency curves in design mode with different design primary and secondary supply temperatures. Fig. 16a shows the overall efficiency of the integrated system. When the primary supply temperature was specified, a lower secondary supply temperature gave a higher overall efficiency level. The reason was that, when the primary supply temperature was specified, a lower secondary supply temperature means a larger temperature drop of the primary side of the heat exchangers in substations, giving a smaller flow and a lower pump power consumption of the primary DH network. When the secondary supply temperature decreased from 55 ℃ to 50 ℃, the efficiency level increased dramatically, especially at lower primary supply temperatures. In contrast, the increase of efficiency level with the decrease of secondary supply temperature from 45 ℃ to 40 ℃ was tiny because of the non-linear relationship between the flow and the pump power. Without considering the losses in the DH network, the CHP plant efficiency curves were at relatively higher levels compared to the overall efficiency curves for the integrated system (see Fig. 16b), but the general trends of the curves were similar.

When the secondary supply temperature was specified, the energy efficiency changed with different primary supply temperatures (see Fig. 16a). With a higher primary supply temperature, the flow rate in the DH netwrok will decrease. The decreased flow rate caused decreased pump power of the DH network. Meanwhile, the heat loss rate will also decrease (see Fig. 13b). All this contributed to the increase of the overall efficiency. However the increase trend of the overall efficiency was slowed down by the fact that higher primary supply temperatures can induce higher back pressure and lower electric power output of the turbine.

In Fig. 16b that there was a efficiency peak for the CHP plant efficiency, and so was it for the overall efficiency. However, these two peaks occurred at different primary supply temperatures. This means that there was a conflict of interest between the CHP plant efficiency and the overall system performance. A relatively higher design supply temperature was preferred according to the overall efficiency. This difference also indicates that it is important to study and analyze on an integrated system level from the primary energy input to the terminal users, other than just researching within a partial scale of the whole system. In the following simulations, only the overall efficiency was considered and analysed.

When the design secondary supply temperature increased, both the CHP plant efficiency and the overall efficiency decreased to lower levels, as shown in Fig. 16b by the curves numbered ① and the curves numbered ②. Meanwhile, the peaks of the CHP plant efficiency and the overall efficiency would all move rightwards with higher primary supply temperatures. This gives us an illumination that the secondary supply temperature should be designed at a rather low level, with the premise that the heat transfer area of radiators does not beyond the heat users' acceptable economic limit (see Fig. 5b).

For a brief summary, the decrease of design secondary supply temperature gave a higher efficiency level, while for the design primary supply temperature there was an optimal value. In the simulations reported below, the design primary and secondary supply temperatures were chosen to be 60 ℃ and 40 ℃, respectively.

4.2. Supply temperature in off-design conditions

As mentioned above, 60 ℃ and 40 ℃ were chosen to be the design primary and secondary supply temperatures, respectively, in this subsection and Section 4.3. The design values in this case is shown in Table 4. When the ambient temperature rises from the design ambient temperature (-30℃), the heat load will decrease. Meanwhile, the primary and secondary supply temperatures can be controlled according to pre-defined curves in operation. For these cases, the simulation was conducted in off-design mode. Fig. 17 shows the energy efficiency performance of the whole system in off-design mode.

In Fig. 17a, the primary supply temperature was kept constant (60 ℃). The overall efficiency decreased slowly first but dramatically later with the increase of secondary supply temperature. For higher ambient temperatures, the overall efficiency curve decreased to lower levels, which means that a smaller heat load would result in a lower overall efficiency. When the ambient temperature was kept constant and the primary supply temperature was decreased/increased from 60 ℃ to 55 ℃/65℃, the efficiency level would be increased/decreased accordingly, shown by Fig. 17b. Considering generally Fig. 17a and Fig. 17b, it was safe to conclude that a lower secondary supply temperature would give relatively higher overall efficiency for the case studied.

When the secondary supply temperature was kept constant (40 ℃), the system performance is shown by Fig. 17c. A higher ambient temperature gave a lower overall efficiency level, which was consistent with the result in Fig. 17a. Meanwhile, there were peak points on the curves in Fig. 17c when the primary supply temperature changed under different ambient temperature conditions. Therefore, the primary supply temperature could be optimized for each ambient temperature in

Table 4: Design parameters of the system with specified design supply temperatures

Term	Temperature (℃)	Pressure (MPa)	Flow (t/h)	Term	Value
Main steam	538	16.7	951.405	Primary supply temperature (℃)	60
Feed water	276.239	20.659	951.405	Secondary supply temperature (℃)	40
Reheat steam to boiler	324.818	3.695	786.881	Turbine power output (MW)	289.893
Reheat steam leaving boiler	538	3.326	786.881	Net power of the whole system (MW)	266.211
Exhaust steam from LPC	65	0.025	640.581	Heat loss of DH network (kW)	5959.21
Steam to condenser for DH	65	0.025	568.306	DH pump power consumption (kW)	14774.3

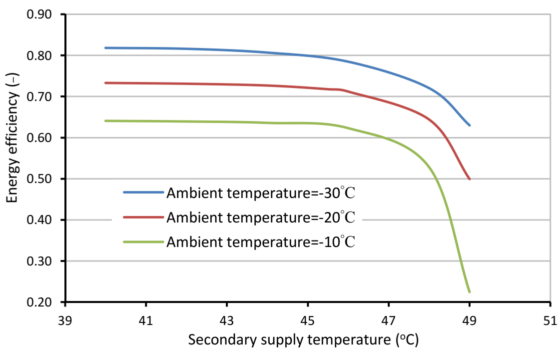

(a) With primary supply temperature kept as 60 ℃

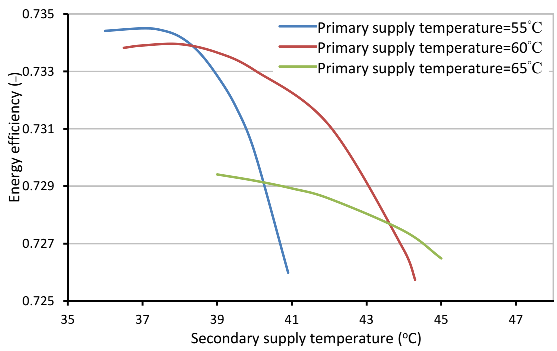

(b) With the ambient temperature of -20℃

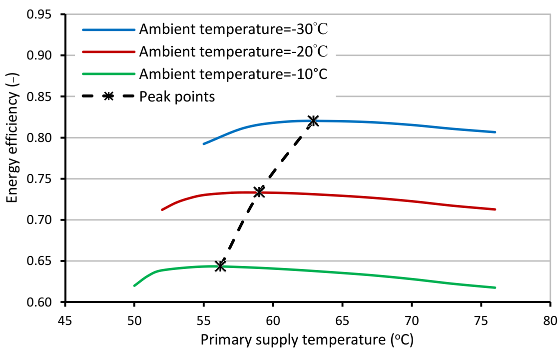

(c) With secondary supply temperature kept at 40℃

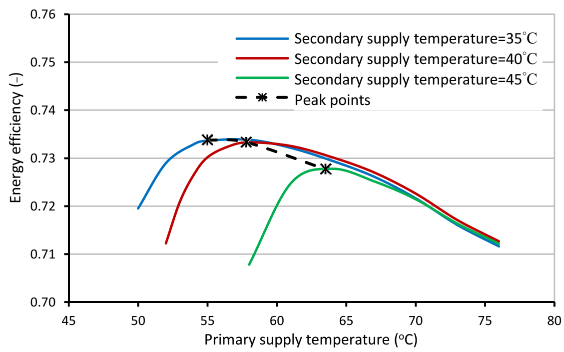

(d) With ambient temperature of -20℃

Figure 17: Overall efficiency curves under off-design conditions with different operational supply temperatures

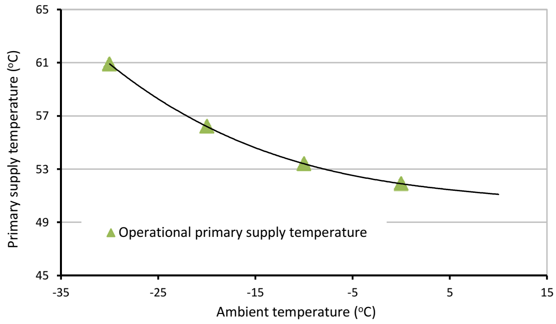

Figure 18: Optimized operational primary supply temperature curve

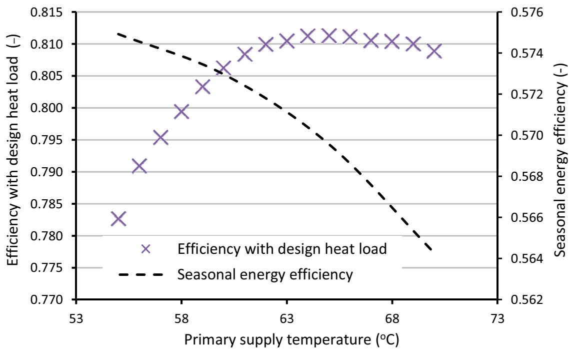

Figure 19: Seasonal energy efficiency study with different design primary supply temperatures

operation. The peak points were fitted as the dashed line in Fig. 17c. For a specified ambient temperature (see Fig. 17d), the peak of the efficiency curve could easily be obtained. It was also easy to find that a lower secondary supply temperature gave a higher peak point, but the trend would slow down for rather low secondary supply temperatures, as shown by the dashed line in Fig. 17d.

To summarize, three basic facts found in this subsection are especially useful. First, the overall efficiency would become lower with a higher ambient temperature. Second, lower secondary supply temperature gave higher overall efficiency. Third and the most important, there was an optimal efficiency point for each heat load condition with regard to different primary supply temperatures (the dashed line in Fig. 17c). The third fact was utilized in the study of the next subsection.

4.3. Seasonal consideration for supply temperatures

The analyses in Sections 4.1 and 4.2 were all evaluated as one state point, either design or off-design, which did not include the system performance during the whole heating season. For the duration of the whole heating season, a heat load curve (see Figs. 14 and 15) was used for the simulation. In order to reflect the influence of design primary supply temperature to the overall efficiency of the whole heating season, seasonal energy efficiency (η_{av}) was used as the system performance indicator in this subsection, as defined in Section 2.

The secondary supply temperature in operation was designed as 40 ℃ and was kept constant in operation. The primary supply temperature was designed as different values within the range from 55 ℃ to 70 ℃. In operation, the primary supply temperature was set as the peak points (the dashed line in Fig. 17c), which was illustrated in Section 4.2. That is to say, for different design primary supply temperatures, there were different optimized curves for operational primary supply temperature, which were fitted by the peak points of the curves in Fig. 17c. The fitted operational curve of primary supply temperature when the design primary supply temperature was set as 55 ℃ is shown by Fig. 18 as an example. In this way, the operational scenarios of the integrated system during the whole heating season could be simulated. When the system outputs under different heat load conditions were multiplied by its corresponding time duration and all the results were summed up, the total overall output of the whole heating season was obtained, so was the total input of the system. Thus the seasonal energy efficiency was obtained for the system with a specified design supply temperature. For different design supply temperatures, the value of the seasonal energy efficiency was different, which is shown by the dashed line in Fig. 19.

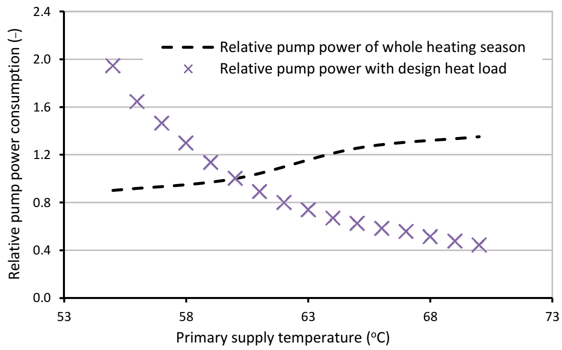

Figure 20: Pump power with different design supply temperatures

For a better comparison, the scatter line in Fig. 19 is exactly the same scatter line in Fig. 16b. In most of the designing practice, the pipeline dimension is highly determined by the design primary supply temperature. The choice of the design supply temperature is always based on the design heat load. However, Fig. 19 shows that a high overall efficiency point under design heat load condition was not always the highest efficiency point when considering the whole heating season performance. From the perspective of the seasonal energy efficiency of the integrated system, a much lower design primary supply temperature is preferred. When the system is designed with a higher primary supply temperature, the overall efficiency in design heat load condition may increase to some extent, but the seasonal energy efficiency of the whole heating period would decrease. The reason for this can be complicated, but two major factors may be dominating. One is the trade-off between the turbine power output in the CHP plant and the pump power consumption in the DH network. The other is that the time duration distribution may have a great influence on the efficiency level of the seasonal energy efficiency, which resulted in the descend trend of the dashed line in Fig. 19. Generally speaking, the primary supply temperature of the heating network should be designed at a rather low temperature level within acceptable investment considerations.

4.4. Pump power consumption of the DH network

Based on the study and analysis in Section 4.3, the pump power consumption with regard to different design primary supply temperature will be presented here. Fig. 20 shows the pump power of the DH network, corresponding to the cases in Fig. 19.

In Fig. 20, the scatter curve was the relationship between the pump power consumption and the different design primary supply temperatures when the heat load was kept constant as design heat load. The pump power when the supply temperature was designed as 60 ℃ was chosen to be the base for the relative value of the scatter curve. This curve shows that, for design heat load, a lower design primary supply temperature gave larger pump power consumption in the DH network. This trend is reasonable because a lower design supply temperature means a larger flow rate in the DH network, noticing that the heat load was specified as design heat load.

If the pump power during the whole heating season was summed up, the seasonal pump power could be obtained. The dashed curve in Fig. 20 was the relative seasonal pump power of the DH network throughout the whole heating season. The base of the relative value was the seasonal pump power with the design supply temperature of 60 ℃. This curve shows that, for the whole heating season, the seasonal pump power decreased with lower design supply temperatures. This trend (the dashed curve in Fig. 20) was quite different from the trend of pump power under design heat load condition (the scatter curve in Fig. 20). The reason was that, for the whole heating season, the largest time duration with regard to different heat load occurred when the ambient temperatur was around 0 ℃ (see Fig. 15). When the ambient temperature was 0 ℃ in operation, the operational supply temperature was much lower than the design value (see Fig. 18). In another word, with a low design supply temperature, the design pump power consumption is high, but this does not contribute much to the seasonal pump power consumption. The seasonal pump power consumption level is related, mainly or to some extent, with the operational supply temperature when the largest duration time occurs. To summarize, it is not always right to relate the low design supply temperature to high pump power consumption, although this is reasonable for design heat load condition. A lower design supply temperature is preferred with consideration of the pump power consumption throughout the whole heating season.

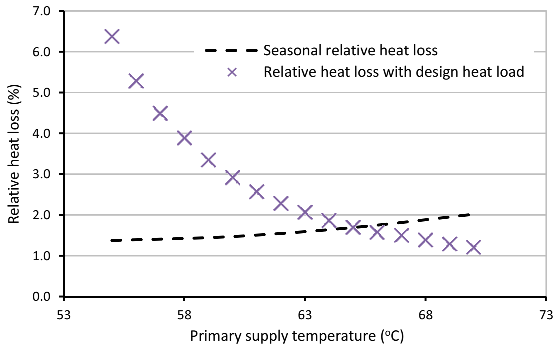

Figure 21: Heat loss with different design supply temperatures

4.5. Heat loss of the DH network

Heat loss of the network is another topic of high interest within the field of DH. For different design supply temperatures, the heat loss would change accordingly. In this subsection the relative DH heat loss with regard to different design supply temperatures will be investigated. The concept of relative heat loss is identical to that mentioned in Section 3.4, meaning the ratio of total heat loss to heat transferred into the DH network. For the seasonal calculation, the summation of the heat loss and the summation of the heat transferred into the DH network were firstly calculated. Then, the ratio of them was obtained as the seasonal relative heat loss.

Fig. 21 presents the results of the heat loss calculations, which also corresponds to the cases in Fig. 19. In Fig. 21, the scatter curve shows the relative heat loss with different design primary supply temperatures under design heat load. For lower design primary supply temperatures, the relative heat loss increased dramatically. This is typical because a lower primary supply temperature means a higher flow rate in the studied case. Furthermore, a higher flow rate means a higher Re value, a higher friction factor, a higher heat transfer coefficient and accordingly a higher heat loss (see Eq. 8 and Eq. 9). The dashed curve in Fig. 21 shows the seasonal relative heat loss with regard to different design primary supply temperatures. The seasonal heat loss decreased with lower design primary supply temperatures, which was different from the trend of the scatter curve. Similar to the trend of the dashed curve in Fig. 20, this was also caused by the time duration distribution with regard to different ambient temperatures throughout the whole heating season (see Fig. 15). That is to say, the effect of high heat loss with a low design supply temperature with design heat load does not contribute much to the seasonal heat loss. Therefore, from the view of seasonal heat loss reduction, lower design supply temperatures are also preferred.

5. Discussion

5.1. Considerations for low temperature district heating

The studies in this paper emphasized on the overall system simulation and the performance of the CHP based DH. The temperature level of the DH network was relatively lower than most of the industry practices, and could be evaluated as low temperature DH. In practical operation, the supply temperature of space heating systems can be considerably decreased to a temperature level below 60 ℃, and for renovated houses it can be supplied all year round with a DH supply temperature of 50 ℃ [32]. Besides, the radiators tends to be oversized in real practice since the designers always want to guarantee that the provided heat is enough, which makes it possible to use further lower operational supply temperatures.

Besides, the operational simulation in this study started out from the minimum design ambient temperature (-30 ℃ in this study). Temperatures below -20 ℃ in this study (80% of the maximum heat load) occur very rarely (see Figs. 14 and 15). If multiple heat sources are used in the DH systems, it may turn out that an electric (or natural gas-fired) heater could be used for the peak heat load for a few hours a year. Then, the optimum design primary supply temperature from the CHP plant should be searched under a lower heat load, which probably will make the design supply temperature even lower.

5.2. Influence of terminal temperature difference of condenser

Since the terminal temperature difference of the condenser was kept constant as 5 ℃, it is necessary to think what if it was changed.

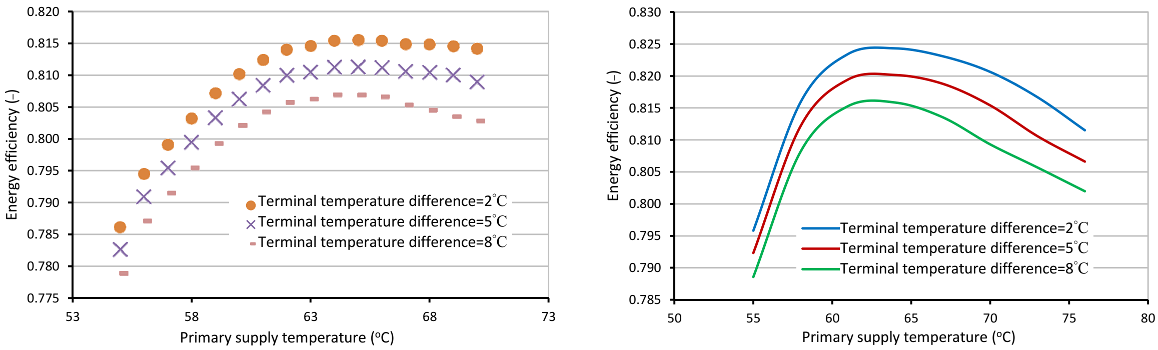

(a) Design mode

(b) Off-design mode

Figure 22: Influence of terminal temperature difference of the condenser to the overall efficiency

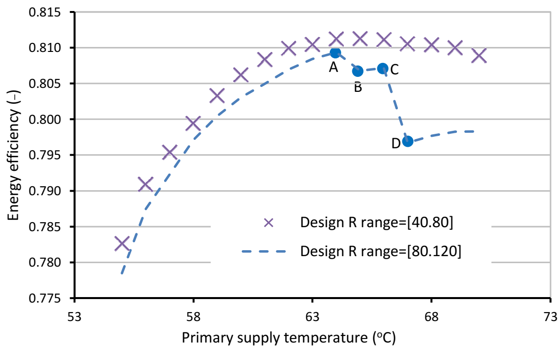

Figure 23: Design overal efficiency with different R range

For design mode, the scatter curve of the overall efficiency in Fig. 16b was taken as the reference case. The curves in Fig. 22a depict the influence caused by the design terminal temperature difference of the condenser. It is easy to find that a higher design terminal temperature difference of the condenser resulted in a lower overall efficiency level. For off-design mode, the very top curve in Fig. 17c was taken as a reference for comparison. The influencing effect was similar to that for the design mode. A 3 ℃ increase of the condenser's terminal temperature difference (both in design and in operation) caused an efficiency drop of 0.5%.

5.3. Choice of specific friction resistance

When designing the pipelines in the DH network, a range of specific friction resistance (R, Eq.7) should be first determined for pipe sizing (sometimes a range of velocity is chosen, which is related to R). A higher R value comes with narrower pipe but higher pump power consumption, so there exists an optimal R range. Although this study did not induce any pipe investment models, the influence of R range to the overall efficiency of the integrated system could be revealed.

Using the scatter curve of the overall efficiency in Fig. 16b as reference, the system efficiency designed with a higher R range was presented by the dashed line in Fig. 23. It is seen that a higher R range gave generally a lower overall efficiency level. Besides, the overall efficiency dropped suddenly when the design supply temperature was increased to some extent. The ladder-like sudden decrease of the efficiency in Fig. 23 was caused by the reduction of the pipe diameter. When the design supply temperature increases, the flow rate for specified heat load would decrease. Lower flow rate would be assigned to a narrower nominal pipe. As mentioned before, a narrow pipe means a higher pump power consumption, which caused the sudden drop of the system efficiency (Point A to B, and Point C to D). It was also found that the efficiency drop from Point A to Point B in Fig. 23 was caused by the diameter change (from 1.2 m to 1.0 m) of a pipe with the length of 1.0×10^3 m, while the larger drop from Point C to Point D was caused by the diameter change (also from 1.2 m to 1.0 m) of a 1.0×10^4 m pipe. This indicated that long distance delivery pipes should be given a lower design R range or a lower design primary supply temperature to avoid the large sudden drop of overall efficiency.

5.4. Future work

The work presented here is the basis of an overall optimization of the integrated CHP based low temperature DH system. The optimum of the system both in design and operation is a more complex matter than the investigations this far have catched up. Besides, investment models have to be considered for further optimization.

6. Conclusions

The CHP plant system was constructed within Ebsilon Professional software. The theoretical model of hydraulic and heat loss calculation of the pipeline in the DH network was set up, based on the fundamentals of heat transfer and fluid mechanics. Furthermore, the heat user and the pipe modules were developed and validated. Meanwhile, the DH network was constructed. Based on the multiscale simulation and analysis, the integrated CHP based DH system was obtained. Moreover, design and operational issues were investigated. The novelties of this article are that both the CHP plant and the DH network were simulated in detail and integrated, the heat and pressure losses of the DH network were coupled in the integrated modeling and the seasonal efficiency was compared with the efficiency in design condition. Several important conclusions were drawn as follows:

- It is important to study and analyze on an integrated system level from the primary energy input to the terminal users, other than just research within a partial scale of the whole system. The integrated model of the CHP based DH system constructed in this paper was capable to carry out the overall system simulation, and was useful for the evaluation of the system performance both in design and operational conditions.
- For design condition, the decrease of design secondary supply temperature of the DH network could give higher overall efficiency level (Fig. 16a), while for different primary supply temperatures there is an optimal design value (Fig. 16b).
- In operation, the overall efficiency would become lower when the heat load decreases. A lower secondary supply temperature of the DH network gives a higher overall efficiency. There is an optimal efficiency point for each heat load condition with regard to different primary supply temperatures (Fig. 17c).
- For seasonal issues throughout the whole heating period, a lower design supply temperature of the DH network means a higher seasonal energy efficiency, although a lower design primary supply temperature usually bring lower overall efficiency in design heat load (Fig. 19). Meanwhile, the pump power consumption of the DH network also show different trends with regard to the design heat load condition and the seasonal condition (Fig. 20). Similar trends also occurred for the heat loss of the DH network (Fig. 21). The seasonal pump power and the seasonal heat loss decrease with a lower design primary supply temperature, which is contrary to the trends for design heat load condition.
- Considering the seasonal energy efficiency, the seasonal pump power consumption and the seasonal heat loss, DH networks with low design supply temperatures are preferred.

Acknowledgments

This work belongs to Subtask C in the project of 'Low temperature district heating for future energy systems' (IEA DHC Annex TS1). The financial support from the National Key Technology R&D Program (2014BAA06B01) and the Joint Funds of the National Natural Science Foundation of China (U1261210) are sincerely acknowledged. Many thanks to the support of Norwegian University of Science and Technology, North China Electric Power University and the support from China Scholarship Council.

Nomenclature

Abbreviations

ACC	air-cooled condenser
CCHP	combined cooling, heat and power
CHP	combined heat and power
DH	district heating
LPC	low pressure cyclinder

Greek Symbols

η_{av}	period energy efficiency, –
η_t	energy efficiency, –

λ thermal conductivity, W/(m·K)

λ_0 thermal conductivity of earth, W/(m·K)

ρ density of water, kg/m^3

τ time, h

τ_0 duration of heating season, h

Latin Symbols

$\dot{G}$ water flow rate in radiator, kg/s

$\dot{Q}$ heat rate/load, W

$\dot{Q}_i$ Input energy of CHP plant, kW

$\dot{Q}_{los}$ rate of heat loss, W

$\dot{Q}_{max}$ maximum heat load, W

$\triangle h$ water enthalpy drop in radiator, J/kg

$\triangle P$ pressure drop, Pa

$\triangle T_{m,r}$ radiator temperature difference, ℃

a, b coefficient parameters of radiator

A_r heat transfer area of radiator, m^2

c_p specific heat at constant pressure, J/(kg·K)

D_1 inner pipe diameter, m

D_2 outer diameter of pipe, m

D_3 outer diameter of insulation, m

f friction factor, -

h outer diameter of insulation, W/(m^2·K)

K roughness of inner pipe surface, m

k_r heat transfer coefficient of radiator, W/(m^2·K)

L length of pipe, m

P_e Power output of CHP plant, kW

R specific frictional resistance, Pa/m

R_1 thermal resistance of insulated pipe, K/W

R_2 thermal resistance of soil over pipe casing, K/W

S shape factor of heat conduction, m

$T_{a,min}$ lowest calculated ambient temperature, ℃

$T_{a,st}$ ambient temperature when heating season starts, ℃

T_a ambient temperature, ℃

$T_{i,p}$ inlet pipe temperature, ℃

$T_{i,r}$ inlet temperature of radiator, ℃

$T_{m,p}$ cross section mean temperature of water in pipe, ℃

T_n indoor temperature needed, ℃

$T_{o,p}$ outlet pipe temperature, ℃

$T_{o,r}$ outlet temperature of radiator, ℃

T_s surface temperature of the earth, ℃

U heat transfer coefficient of insulated pipe, W/(m^2·K)

v velocity of water, m/s

z buried depth of pipe centerline, m

Subscripts

a ambient

c pipe casing

i inlet

m mean

max maximum

min minimum

n needed

o outlet

p pipe

r radiator

w water

References

[1] BP Group. Bp statistical review of world energy june 2014. Technical report, BP company, 2013.

[2] John Harold Horlock. *Combined Heat and Power*. Pergamon Books Inc., Elmsford, NY, 1987.

[3] European Parliament and Council of European Union. Directive 2004/8/ec of the european parliament and the council of 11 february 2004 on the promotion of cogeneration based on a

useful heat demand in the internal energy market and amending directive 92/42/eec. *Official Journal of the European Union*, L52:50–60, 2004.

[4] ZG Sun, RZ Wang, and WZ Sun. Energetic efficiency of a gas-engine-driven cooling and heating system. *Applied thermal engineering*, 24(5):941–947, 2004.

[5] Gianfranco Chicco and Pierluigi Mancarella. Trigeneration primary energy saving evaluation for energy planning and policy development. *Energy Policy*, 35(12):6132–6144, 2007.

[6] N Fumo, PJ Mago, and LM Chamra. Cooling, heating, and power energy performance for system feasibility. *Proceedings of the Institution of Mechanical Engineers, Part A: Journal of Power and Energy*, 222(4):347–354, 2008.

[7] Ivar S Ertesvåg. Exergetic comparison of efficiency indicators for combined heat and power (chp). *Energy*, 32(11):2038–2050, 2007.

[8] Zhi-Ping Song. Total energy system analysis of heating. *Energy*, 25(9):807–822, 2000.

[9] HI Onovwiona and VI Ugursal. Residential cogeneration systems: review of the current technology. *Renewable and sustainable energy reviews*, 10(5):389–431, 2006.

[10] DW Wu and RZ Wang. Combined cooling, heating and power: a review. *progress in energy and combustion science*, 32(5):459–495, 2006.

[11] Joel Hernández-Santoyo and Augusto Sánchez-Cifuentes. Trigeneration: an alternative for energy savings. *Applied Energy*, 76(1):219–227, 2003.

[12] Gianfranco Chicco and Pierluigi Mancarella. From cogeneration to trigeneration: profitable alternatives in a competitive market. *Energy Conversion, IEEE Transactions on*, 21(1):265–272, 2006.

[13] Hirohisa Aki, Shigeo Yamamoto, Junji Kondoh, Tetsuhiko Maeda, Hiroshi Yamaguchi, Akinobu Murata, and Itaru Ishii. Fuel cells and energy networks of electricity, heat, and hydrogen in residential areas. *International Journal of Hydrogen Energy*, 31(8):967–980, 2006.

[14] N Perdikaris, KD Panopoulos, Ph Hofmann, S Spyrakis, and E Kakaras. Design and exergetic analysis of a novel carbon free tri-generation system for hydrogen, power and heat production from natural gas, based on combined solid oxide fuel and electrolyser cells. *International Journal of Hydrogen Energy*, 35(6):2446–2456, 2010.

[15] Francisco Toja-Silva and Antonio Rovira. A first and second thermodynamics law analysis of a hydrogen-fueled microgas turbine for combined heat and power generation. *Journal of Engineering for Gas Turbines and Power*, 136(2):021501, 2014.

[16] Henrik Lund. Large-scale integration of wind power into different energy systems. *Energy*, 30(13):2402–2412, 2005.

[17] Brian Leif Hanrahan, Gordon Lightbody, Lawrence Staudt, and Paul G Leahy. A powerful visualization technique for electricity supply and demand at industrial sites with combined heat and power and wind generation. *Renewable and Sustainable Energy Reviews*, 31:860–869, 2014.

[18] Mohammad Reza Ranjbar, Mohsen Mohammadian, et al. Economic analysis of hybrid system consists of fuel cell and wind based chp system for supplying grid-parallel residential load. *Energy and Buildings*, 68:476–487, 2014.

[19] Sheng Li, Jun Sui, Hongguang Jin, and Jianjiao Zheng. Full chain energy performance for a combined cooling, heating and power system running with methanol and solar energy. *Applied Energy*, 112:673–681, 2013.

[20] W Yagoub, P Doherty, and SB Riffat. Solar energy-gas driven micro-chp system for an office building. *Applied thermal engineering*, 26(14):1604–1610, 2006.

[21] Ye Huang, DR McIlveen-Wright, Sina Rezvani, MJ Huang, YD Wang, AP Roskilly, and NJ Hewitt. Comparative techno-economic analysis of biomass fuelled combined heat and power for commercial buildings. *Applied Energy*, 112:518–525, 2013.

[22] Christian Bang-Møller, Masoud Rokni, Brian Elmegaard, Jesper Ahrenfeldt, and Ulrik Birk Henriksen. Decentralized combined heat and power production by two-stage biomass gasification and solid oxide fuel cells. *Energy*, 58:527–537, 2013.

[23] Behnaz Rezaie and Marc A Rosen. District heating and cooling: Review of technology and potential enhancements. *Applied Energy*, 93:2–10, 2012.

[24] Svend Frederiksen and Sven Werner. *District heating and cooling*. studentlitteratur, 2013.

[25] Henrik Gadd and Sven Werner. Heat load patterns in district heating substations. *Applied Energy*, 108:176–183, 2013.

[26] Henrik Gadd and Sven Werner. Daily heat load variations in swedish district heating systems. *Applied Energy*, 106:47–55, 2013.

[27] Urban Persson and Sven Werner. District heating in sequential energy supply. *Applied Energy*, 95:123–131, 2012.

[28] Urban Persson and Sven Werner. Heat distribution and the future competitiveness of district heating. *Applied Energy*, 88(3):568–576, 2011.

[29] Patrick Lauenburg. *Improved supply of district heat to hydronic space heating systems*. PhD thesis, Lund University, 2009.

[30] Jonas Gustafsson, Jerker Delsing, and Jan van Deventer. Improved district heating substation efficiency with a new control strategy. *Applied Energy*, 87(6):1996–2004, 2010.

[31] Jonas Gustafsson, Jerker Delsing, and Jan Van Deventer. Experimental evaluation of radiator control based on primary supply temperature for district heating substations. *Applied Energy*, 88(12):4945–4951, 2011.

[32] Marek Brand and Svend Svendsen. Renewable-based low-temperature district heating for existing buildings in various stages of refurbishment. *Energy*, 62:311–319, 2013.

[33] Henrik Lund, Sven Werner, Robin Wiltshire, Svend Svendsen, Jan Eric Thorsen, Frede Hvelplund, and Brian Vad Mathiesen. 4th generation district heating (4gdh): Integrating smart thermal grids into future sustainable energy systems. *Energy*, 68:1–11, 2014.

[34] Pei Feng Li, Zhihua Ge, Zhiping Yang, Yuyong Chen, and Yongping Yang. District heating mode analysis based on an air-cooled combined heat and power station. *Entropy*, 16(4):1883–1901, 2014.

[35] Zhihua Ge, Xiaoze Du, Lijun Yang, Yongping Yang, Yanlei Li, and Yansheng Jin. Performance monitoring of direct air-cooled power generating unit with infrared thermography. *Applied Thermal Engineering*, 31(4):418–424, 2011.

[36] Hemin Hu, Xiaoze Du, Lijun Yang, Yingyan Zhou, and Yongping Yang. Pod-based modeling on thermal-flow characteristics for air-cooled condenser of power plant. *International Journal of Thermal Sciences*, 76:273–281, 2014.

[37] STEAG Energy Services GmbH. *EBSILON Professional for engineering and designing energy and power plant systems*. $http://www.steag-systemtechnologies.com/ebsilon_professional+M52087573ab0.html$, accessed on July 31, 2014.

[38] W Wagner, JR Cooper, A Dittmann, J Kijima, H-J Kretzschmar, A Kruse, R Mares, K Oguchi, H Sato, I Stocker, et al. The iapws industrial formulation 1997 for the thermodynamic properties of water and steam. *Journal of Engineering for Gas Turbines and Power*, 122(1):150–184, 2000.

[39] David H Cooke. Modeling of off-design multistage turbine pressures by stodola's ellipse. In *Energy Incorporated PEPSE user's group meeting*, 1983.

[40] Hans Peter Wolf. *Accompanying material for the EBSILON Professional training course*. STEAG, 2012.

[41] Damao Xu, Yan Ke, and Shiyong Wang. Universal method for calculating the power/back-pressure characteristics of a steam turbine and its applications. *Journal of Engineering for Thermal Energy and Power*, 25(6):605–608, 2010. (in Chinese).

[42] Lihua Zong. Thermal performance analysis of concrete embedded plastic pipe radiant floor heating. *Gas & Heat*, 20(1):18–20, 2000. (in Chinese).

[43] John Siegenthaler. *Modern hydronic heating: for residential and light commercial buildings.* Cengage Learning, 2011.

[44] Frank P Incropera, Adrienne S Lavine, Theodore L Bergman, and David P DeWitt. *Principles of heat and mass transfer.* Wiley, 2013.

[45] Ping He and Gang Sun. *Heating engineering.* Architecture & Building Press, 2009. (in Chinese).

[46] Logstor. *Logstor calculator 2.1. http : //calc.logstor.com/*, accessed on July 31, 2014.

[47] Max Wolf and Hellmuth Junge. Belastungskurven und dauerlinien in der elektrischen energiewirtschaft. In Max Wolf, editor, *Enzyklopädie der Energiewirtschaft*, volume 2, Berlin, 1959. Springere-Verlag.

[48] Andrzej Ziębik and Paweł Gładysz. Optimal coefficient of the share of cogeneration in district heating systems. *Energy*, 45(1):220–227, 2012.

List of Tables

List of Figures